Biophysics and Physicobiology

Review Article (Invited)

Quantum nanodiamonds for sensing of biological quantities: Angle, temperature, and thermal conductivity

Shingo Sotoma[1], Hirotaka Okita[1], Shunsuke Chuma[1,2], Yoshie Harada[1,3]

[1] Institute for Protein Research, Osaka University, Osaka 565-0871, Japan

[2] Department of Biological Sciences, Graduate School of Science, Osaka University, Osaka 560-0043, Japan

[3] Center for Quantum Information and Quantum Biology, Osaka University, Osaka 565-0871, Japan

Measuring physical quantities in the nanometric region inside single cells is of great importance for understanding cellular activity. Thus, the development of biocompatible, sensitive, and reliable nanobiosensors is essential for progress in biological research. Diamond nanoparticles containing nitrogen-vacancy centers (NVCs), referred to as fluorescent nanodiamonds (FNDs), have recently emerged as the sensors that show great promise for ultrasensitive nanosensing of physical quantities. FNDs emit stable fluorescence without photobleaching. Additionally, their distinctive magneto-optical properties enable an optical readout of the quantum states of the electron spin in NVC under ambient conditions. These properties enable the quantitative sensing of physical parameters (temperature, magnetic field, electric field, pH, etc.) in the vicinity of an FND; hence, FNDs are often described as "quantum sensors". In this review, recent advancements in biosensing applications of FNDs are summarized. First, the principles of orientation and temperature sensing using FND quantum sensors are explained. Next, we introduce surface coating techniques indispensable for controlling the physicochemical properties of FNDs. The achievements of practical biological sensing using surface-coated FNDs, including orientation, temperature, and thermal conductivity, are then highlighted. Finally, the advantages, challenges, and perspectives of the quantum sensing of FND are discussed. This review article is an extended version of the Japanese article, In Situ Measurement of Intracellular Thermal Conductivity Using Diamond Nanoparticle, published in SEIBUTSU BUTSURI Vol. 62, p.122-124 (2022).

Key words: biosensing, cell, fluorescent nanodiamonds, nitrogen vacancy, quantum sensor

---

◀ *Significance* ▶

Recently, the involvement of various physical factors such as temperature in biological phenomena has been reported. Fluorescent nanodiamonds are excellent sensors for measuring physical factors, both in vitro and in vivo. This review provides basic information on the functionality of fluorescent nanodiamonds and interesting cell-specific findings by measuring the fluidity of cell membranes and the temperature of single living cells using fluorescent nanodiamonds. We hope that this review will draw more attention to the influence of physical phenomena on life processes and more seamlessly link biology and physics, thereby furthering development within both fields.

Corresponding authors: Shingo Sotoma, Institute for Protein Research, Osaka University, 3-2 Yamadaoka, Suita, Osaka 565-0871, Japan. ORCID iD: https://orcid.org/0000-0001-9528-471X, e-mail: ssotoma@protein.osaka-u.ac.jp; Yoshie Harada, Institute for Protein Research, Osaka University, 3-2 Yamadaoka, Suita, Osaka 565-0871, Japan. ORCID iD: https://orcid.org/0000-0003-2249-5553, e-mail: yharada@protein.osaka-u.ac.jp

Introduction

Quantum sensing is a new area of quantum technology treating well-controlled quantum systems which has recently become a distinct and rapidly growing research area within quantum science and technology [1]. Nitrogen-vacancy centers (NVCs) in diamond crystals have emerged as solid-state quantum sensors due to their outstanding ability to sense various physical quantities such as magnetic field, electric field, and temperature [1-3]. When NVCs are embedded inside nanosized diamond particles, the nanoparticles serve as a quantum sensor that allows the measurement of these parameters at the nano scale. Nanodiamond (ND) containing NVCs, called fluorescent nanodiamonds (FNDs), were developed by Chang et al. in 2005 [4]. Most of their early applications were the fluorescent labeling of biomolecules and cells by taking advantage of their exceptional photostability and low cytotoxicity [5,6]. However, interest in FNDs has shifted in recent years towards biosensing applications [7-9]. The quantum state of the electron spin inside an NVC can be determined from the light emitted from the NVC (optically detected magnetic resonance (ODMR)), and ODMR is sensitive to the environment surrounding the NVC [10]. Therefore, if FND can be applied to cellular measurements, it would be possible to quantitatively measure various physical quantities, chemical reactions, and structural changes in the intracellular nanoregion, which are difficult to measure using conventional techniques. Because of these properties, FNDs are often described as "quantum sensors".

Many research groups have achieved unique nanosensing applications using FND quantum sensors [7-9]. Fujisaku et al. demonstrated that nanodiamonds serve as nanometric pH sensors [11]. In their study, they reported that FND with carboxy groups served as a sensor from pH 3 to 7 and cysteine-modified FND from pH 7 and 11 through relaxation time (T_1) measurement. Ermakova et al. reported the detection of metallo-protein (ferritin) molecules by observing a significant reduction in both coherence and spin-lattice relaxation times [12]. The result confirmed that the presence of very few ferritin molecules (~10) has a strong and quantifiable impact on the spin properties of NVC, thus demonstrating the potential for the sensing of a few biological molecules using single FNDs. Barton et al. developed a hybrid system consisting of FND and nitroxide spin label [13]. The system successfully monitored the redox reaction of the L-ascorbate anion to dehydroascorbic acid with a resolution down to ~10 spins per FND. Schirhagl et al. monitored cellular metabolic activity in single mitochondria and sensing of free radicals in primary human dendritic cells by monitoring the T_1 of NVCs in FND [14,15]. Miller et al. developed an ultrasensitive detection system for a COVID-19 lateral flow immunoassay [16]. The group modulated the fluorescence intensity of FNDs using a microwave field to improve detection sensitivity by separating the FND florescence signal and background autofluorescence. This method achieved a 10^5-fold increase in sensitivity compared with the conventional lateral flow assay based on gold nanoparticles.

In parallel with these studies, our group has been developing an ODMR microscope to measure the orientation and temperature in the nanometric region using FNDs and applying these techniques to living cells [17-23]. Therefore, in this paper, we review the properties of FNDs with NVCs, surface chemical modification required to make FNDs water-soluble and functional, and their state-of-the-art quantum sensing applications for biomolecules and living cells, including orientation, temperature, and thermal conductivity.

Nitrogen-Vacancy Center and Optically Detected Magnetic Resonance

NVC is a crystal defect in a diamond composed of a nitrogen atom and a vacancy center adjacent to each other (Figure 1A) [24,25]. NVCs have two charge states: neutral (NV^0, electron spin: $S = 1/2$) and negatively charged (NV^-, $S = 1$) [24]. An energy diagram of NV^- is depicted in Figure 1B [26]. Both NVCs emit fluorescence in the near-infrared region when excited by green light (Figure 1C); hence, nanodiamonds containing NVCs are often called FNDs [4,27]. Photobleaching of fluorescent molecules (e.g. dyes and proteins) is a major concern in fluorescence imaging, which is speculated to be caused by the degradation of the fluorophores by the irradiation of excitation light. Because NVC fluorophores are deeply embedded inside robust diamond crystal structure and thus highly structurally stable, FND fluorescence shows no photobleaching [4]. Besides, it has been reported that FNDs with a particle size of 100 nm, which are widely used in biomedical applications, do not exhibit photoblinking [28]. However, it should be noted that the blinking FNDs have been reported as the particle size decreases because NV centers become more susceptible to surface effects [29,30]. The stable fluorescence renders FNDs ideal probe for long-term and single-molecule imaging applications [5,6].

Zero-phonon lines of NV^0 and NV^- are observed at 575 and 637 nm, respectively. Among these NVCs, special attention is paid to NV^- centers because of their unique magneto-optical properties (Figure 1B) [5,6]. The ground state of NV^- is a spin triplet, and the spin sublevels ms = 0 and ms = ±1 are split by zero-field splitting D (ca. 2870 MHz), with the spin sublevels ms = ±1 degenerating in the absence of an external magnetic field. Microwave (MW) irradiation at this frequency induces electron spin magnetic resonance between the ms = 0 and ms = ±1 spin levels, resulting in reduced fluorescence emission due to spin-dependent intersystem crossing. The optical readout of these spin quantum states is known as the ODMR (Figure 1D) [1,2,24,31]. The spin Hamiltonian, which describes the total energy of the quantum

system of the ground state of the NVC, can be written as (1).

$$H = g\mu_B B S + D\left[S_z^2 - \frac{1}{3}S(S+1)\right] + E\left(S_x^2 - S_y^2\right) \tag{1}$$

Here, B is the magnetic field strength, μ_B is the Bohr magneton, S is the effective electron spin (S = 1 for a triplet state), g is the electronic g-tensor, D is the fine-structure zero-field splitting, and E is the strain-induced splitting coefficient.
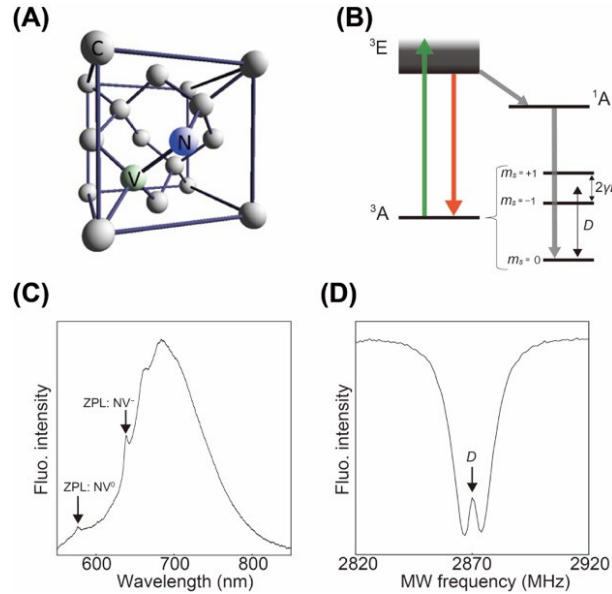
Figure 1 (A) Structure of an NVC in diamond crystal. C: carbon atom, N: nitrogen atom, V: vacancy. (B) Energy level diagram of NV⁻. D is zero-field splitting and $2\gamma B$ is the Zeeman splitting, where γ is the NV gyromagnetic ratio. (C) Fluorescence and (D) ODMR spectra of FNDs excited at 532 nm. ZPL: Zero-phonon line.

Angular Sensing

   NV centers function as sensors that can measure external magnetic fields [32,33]. In the presence of an external magnetic field, the degeneracy of the ms = ±1 spins is broken, and the energy is split. The width of this splitting depends on the angle between the magnetic field vector and the NV axis. In other words, if the intensity and direction of the external magnetic field are known, the angle of the NV center towards the magnetic field can be determined using tomographic vector magnetometry. The advantage of angle measurement using FND is that the rotational motion of a single molecule in a living biological system can be measured, which is technically difficult using other techniques. An early study demonstrated the tracking of a single FND containing a single NVC in live HeLa cells [34]. Recently, Igarashi et al. achieved the tracking of three-dimensional rotational motion (roll-pitch-yaw, θ-φ-σ) of an FND with ensemble NV centers [21]. The group developed an orthogonally aligned three-axis magnet system (Figure 2A and 2B), allowing the generation of a magnetic field of arbitrary magnitude and direction, thus enabling the measurement of the orientation for single (Figure 2C and 2D) and ensemble NVCs (Figure 2E and 2F). Using this equipment, they verified that the orientations of nanodiamonds can be determined with an angular uncertainty of ±3° at 1.7 s time resolution.

Temperature Sensing: ODMR

   In the ODMR spectrum (Figure 3A), microwave-frequency-dependent changes in NV⁻ fluorescence intensity provided valuable information, including the sample temperature. By monitoring the temperature-dependent shift of the zero-field splitting D, it is possible to measure the temperature around the FNDs. Acosta et al. first demonstrated that NV⁻ could serve as a temperature sensor[35]. They measured the temperature-dependent shift in D from 280 to 330 K for an NV⁻ center ensemble at 0.01–15 ppm and reported a thermal shift of $\Delta D/\Delta T = -75$ kHz/K (Figure 3B).

   For measurements of biologically relevant temperatures, it is problematic for biological factors beyond temperature to influence the temperature-sensing ability of FNDs. However, Sekiguchi et al. demonstrated that the thermosensing ability of FNDs is barely influenced by environmental factors including pH, ion concentration, viscosity, molecular interactions, and the presence of organic solvents [17]. Thus, FNDs can serve as robust temperature sensors inside single cells.
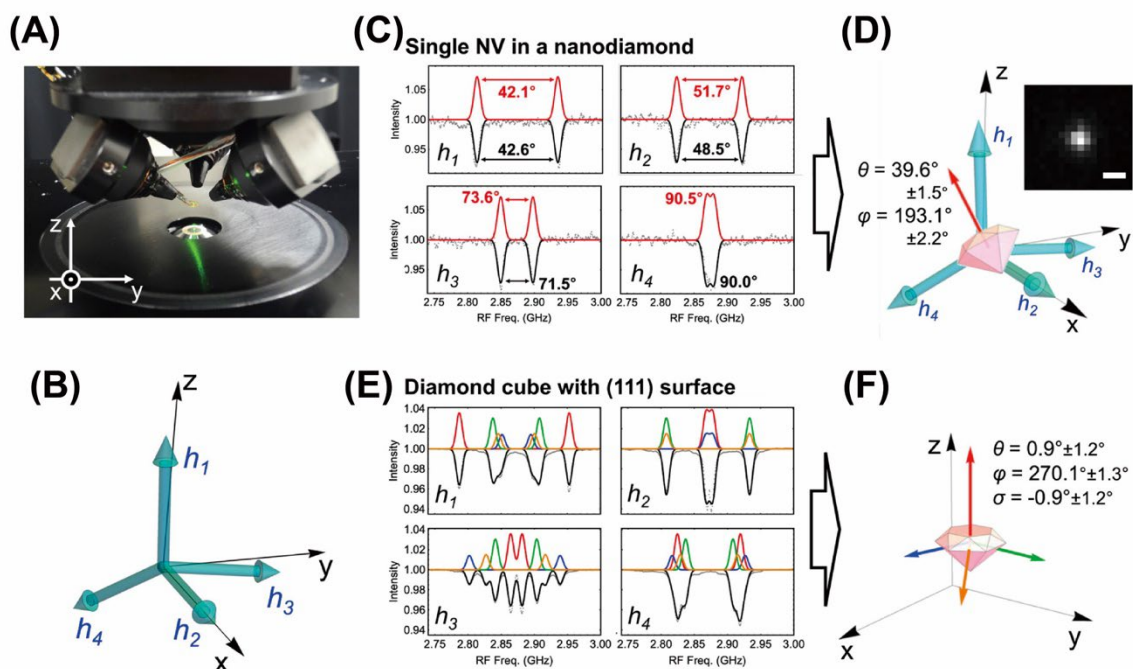
Figure 2 Proof-of-principle experiment for orientation determination by ODMR. (A) The orthogonally aligned three-axis magnet system used to generate the arbitrary external magnetic field. (B) The four magnetic field directions used in this proof-of-principle experiments (blue arrows). (C) Typical ODMR spectra of a nanodiamond containing a single NV center acquired with each external magnetic field. The angles of the N−V axis relative to the applied magnetic field derived from the Zeeman split widths are indicated. Gray dots, raw data; downward black lines, best-fit curves obtained by fitting each spectrum independently; upward red lines, best-fit curves obtained by considering the geometrical limitation among the four angles. (D) Direction of the N−V axis in a 50 nm nanodiamond (inset; scale bar, 1 μm) calculated by considering the geometrical limitation. (E) Typical ODMR spectra of a 1 mm diamond cube with a (111) surface acquired with each external magnetic field. Gray dots, raw data; downward black lines, fit to a theoretical model; upward colored lines, signals attributed to the NV centers depicted with corresponding colors in (F). (F) The four directions of N−V axes in the diamond cube (colored arrows). The Tait−Bryan angles shown are relative to the default orientation explained in the main text. Modified with permission from Ref 21.
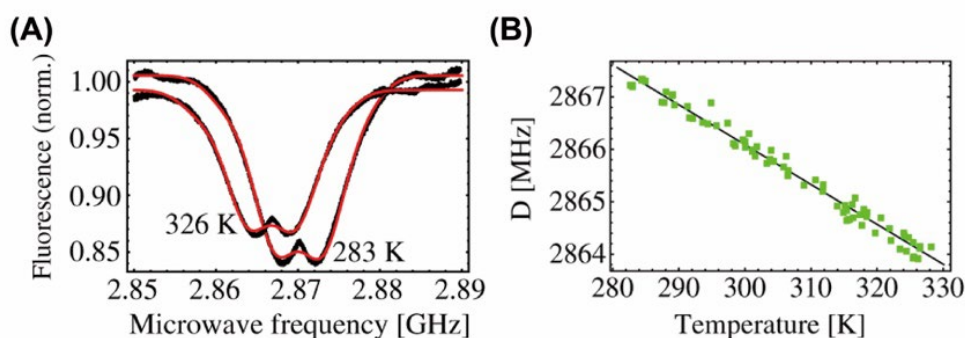

Figure 3 (A) Temperature-dependent shifts of an ODMR spectrum. (B) Frequency shifts of the ODMR peak center around 280–330 K. Modified with permission from Ref 35.

Temperature Sensing: All-optical

The fluorescence spectra of NV⁻s in FNDs were characterized by a zero-phonon line (ZPL) at 637 nm (Figure 1C), whose wavelength shifts can be used to measure the temperature [36]. It is also possible to monitor the change in ZPL height by referencing its phonon sideband using a ratiometric technique developed by Plakhotnik et al. [37]. Such all-optical methods are preferable for bioapplications because they do not require a metal wire to induce the MW frequency, which must be placed close to the FNDs for the ODMR method. The temperature-dependent change in the ZPL position is relatively small (0.015 nm/K^{-1}); however, the accuracy of the temperature measurements can reach sub-kelvin levels owing to the lack of FND fluorescence photobleaching. For example, Hui et al. reported that the temperature sensitivities using ZPL shifts and height changes of FNDs embedded in poly(2-hydroxyethyl methacrylate) (PHEMA) were 0.46–1.1 and 0.15–0.62 K Hz$^{-1/2}$, respectively, over the temperature range of 35–120 °C (Figure 4) [38].
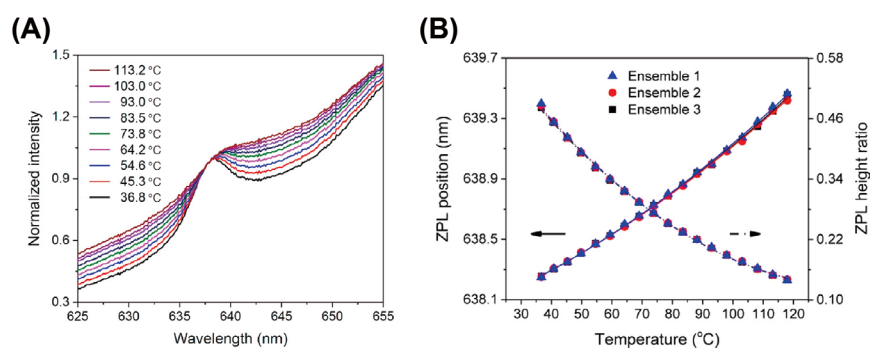

Figure 4 (A) Comparisons of the fluorescence spectra in the ZPL region of NV⁻ centers in PHEMA-embedded FNDs at 36.8–113.2 °C. The spectra were normalized to the intensity at 638.161 nm. (B) Changes in ZPL position and height ratios over 35–120 °C for three representative FND ensembles embedded in the PHEMA films. Curves represent the best fits of the experimental data using second-order polynomials. Modified with permission from Ref 38.

Surface Coating of FNDs

The surfaces of FNDs are hydrophobic and easily precipitate in solutions containing salts [39]. Surface coating is an effective solution to this problem, improving dispersibility and adding other biological functions [40,41]. Commonly used coatings are shown in Figure 5. Non-covalent coatings include bovine/human serum albumin (BSA/HSA), polyethyleneimine (PEI), and lipids, while covalent coatings include photocrosslinked lipids (PCL), polydopamine (PDA), silica, and hyperbranched polyglycerol (HPG). All coatings except PDA were considered to have little effect on the fluorescence and ODMR properties of the FNDs.

Protein coating is a simple method to control the dispersity and nonspecific adsorption of FNDs, whose effectiveness is not as high as that of lipid and HPG coatings. Additionally, the presence of various functional groups derived from proteins on the coated FND surface, which results in a nonuniform surface chemical structure, should be noted. The preparation of FND and protein is quite simple, for example, mixing FNDs and proteins (BSA or HSA) in aqueous solution to afford hybrids [42]. By using biotinylated BSA for synthesis, selective binding of FNDs to avidin molecules can be achieved [16]. Tzeng et al. used FND-BSA composites for stimulated emission depletion (STED) microscopy and demonstrated the imaging of individual particles in HeLa cells at a resolution of 39 nm [43]. Epperla et al. employed FND, BSA, and green fluorescent protein hybrids (FND-BSA-GFP) to continuously monitor intercellular transportation through membrane-tunneling nanotubes over 10 min [44]. Highly stable FND-protein hybrids with specific cell labeling and targeting were demonstrated by Chang et al. [45]. They designed FND and glycosylated BSA molecules formed by chemical modification of BSA with carbohydrates and showed a high targeting ability to HepG2 and human liver cancer cells. Su et al. reported a unique composite comprising FND and luciferase for fluorescence/luminescence multimodal imaging [46].

PEI coating is another method of noncovalent coating with negatively charged FND and positively charged PEI via electrostatic interactions [47,48]. Similar to protein coatings, the coating method is simple [48]. The resulting FND-PEI has a positive zeta potential and can be used as a carrier for negatively charged molecules such as DNA. Petrakova et al. imaged intracellular DNA transfection in real time by monitoring the fluorescence intensity changes of FND, which are significantly influenced by the surface charge state [49].

A simple lipid-coating method was developed by Hsieh et al. taking advantage of the Ouzo effect [50]. This method does not require complex organic synthesis techniques. The lipid-coated FNDs showed high dispersity and strongly
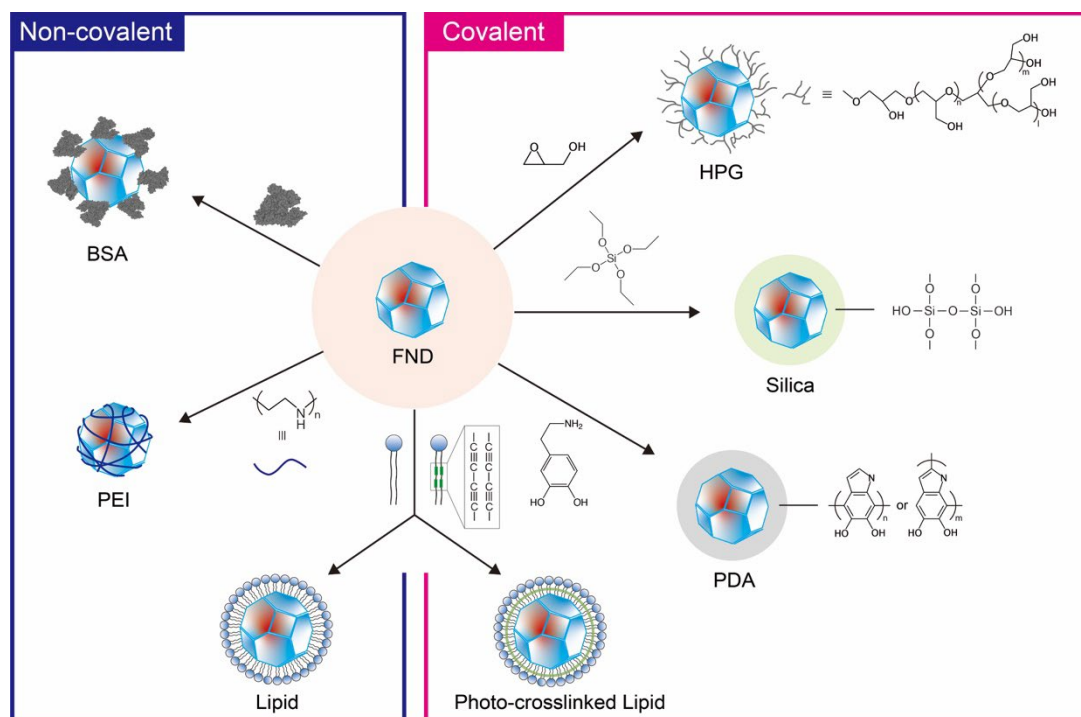
Figure 5 Surface coating of FND.

reduced nonspecific protein adsorption on the FND surface; thus, lipid-coated FND with anti-CD44 antibody realizes highly selective targeting of CD44 on HeLa cell membranes. Further improvement of the structural stability is possible by coating diacetylene-containing lipids and subsequent UV irradiation, affording photocrosslinked lipid-coated FNDs [51]. The structure of lipids on bare FND is considered to be a monolayer or a mixture of mono/bilayer. Vavra et al. successfully developed a single phospholipid bilayer on FNDs with thin silica shells. The group showed sensitive detection of the local magnetic field fluctuation generated by Gd_3^+-labeled phospholipids through the T_1 of NVC [52]. The group reported that the supported phospho-lipid bilayer interface increased the detection sensitivity by approximately one order of magnitude. Improved cell uptake of FND-lipid hybrids into yeast cells and their fate during cell division have been reported by Morita et al. [53].

Zeng et al. made an early demonstration of PDA coating on FND [54]. The synthesis was simple: FND and dopamine molecules were mixed in Tris-HCl (0.01 M, pH = 8.5) solution and vigorously stirred overnight to afford FND-PDA. The catechol/quinone groups on the PDA layer serves as a versatile platform for further chemical reactions. The group further demonstrated the direct growth of Ag nanoparticles from [Ag (NH$_3$)$_2$] OH and their hybridization with gold nanorods. FND-PDA has poor solubility in water; however, Jung et al. reported that FND-PDA and polyethylene glycol conjugation enhanced colloidal stability in physiological solutions [55]. The group demonstrated long-term high-resolution single-molecule tracking of DNA-tethered FND-PDA. It is important to note that PDA absorbs light of all wavelengths and thus weakens the fluorescence intensity of the FNDs in a thickness-dependent manner [22,55].

Silica coating affords nanoparticles with high colloidal stability over a wide pH range, and the surface silanol groups allow further chemical functionalization. Bumb et al. attempted to coat FND with silica [56]. FND and tetraethyl orthosilicate (TEOS) were first trapped in multilamellar vesicles ranging from 500 to 10000 nm in size. The vesicles were subsequently broken by ultrasonication into small unilamellar vesicles, and TEOS was then converted to silica on the FND surface by triethylamine. The FND-silica can conjugate to biomolecules, and based on the coating, they demonstrated 3D single tracking of FNDs tethered to DNA with high spatiotemporal resolution. Cigler et al. developed a different approach to silica encapsulation [57]. TEOS was directly polymerized on the surface of polyvinylpyrrolidone-coated FNDs and further modified with a polymer to introduce a click chemistry interface. The group achieved selective targeting of LNCaP (adenocarcinoma) and U87MG (glioblastoma) cells. Chu et al. prepared round-shaped FNDs with a thick silica layer and showed that the shape of the nanoparticles influences their fate after cell internalization [58]. They were not observed to directly penetrate the plasma membranes, but could penetrate the endosomal membranes easily. On the other hand, a sharp-shaped FNDs, regardless of their surface chemistry, size, or composition, could pierce the membranes of endosomes that carry them into the cells and escape to the cytoplasm.

Ring-opening polymerization of glycidol to synthesize hyperbranched polyglycerol (HPG) on the surface of nanoparticles is a facile and scorable technique for obtaining nanoparticles with excellent dispersity and functionality [59]. An early study of HPG-modified ND was reported by Zhao et al.; NDs and glycidols reacted together under a nitrogen atmosphere at 140 °C for 24 h, yielding ND-HPG [60]. The method is simple and does not require any metal catalysts or initiators distinct from atom transfer radical polymerization (ATRP) for polymer grafting. The produced ND-HPG showed strong resistance to aggregation in salt-containing, high-, or low-pH solutions [60,61]. OH groups on HPG can be relatively easily functionalized by chemical/biological molecules, and several advanced applications have been reported so far, including selective molecular targeting [39], single particle tracking [62], cancer imaging[63] and drug delivery [64]. The mechanism of the ring-opening reaction is the consecutive nucleophilic reaction between a COOH or OH group and a carbon atom in the epoxy group. Based on this finding, Sotoma et al. reported that HPG can be easily functionalized with COOH [65], trimethylammonium (TMA) [66], or alkyne groups [62] in a one-pot reaction with bare FND. The alkyne group-modified FND-HPG allowed the copper-catalyzed click reaction in an aqueous solution. This group successfully tracked membrane protein dynamics in living cells for over ten hours [62].

Angular

The functions of biomolecules depend significantly on their structures and structural changes. Structural changes can be completely described in terms of transition (x-y-z) and rotation (θ–φ–σ). Although 3-D transitional motion can be tracked with 1 nm accuracy by fluorescence imaging techniques [67], tracking the rotational motion of biomolecules in living cells with sufficient accuracy has not yet been achieved.

McGuinness et al. demonstrated that the absolute orientation of FNDs can be tracked independently using the vector dependence of the NV center on the magnetic field, achieving a precision of less than 1 [34]. They demonstrated four-dimensional tracking (position and orientation) of an FND in a HeLa cell over 3 h, proving the significant potential of FNDs for intracellular rotational tracking applications. Adopting a three-axis magnet system, Igarashi et al. tracked the three-dimensional rotational motion of FND in biological systems, including the rotational motion of F1ATP-ase, membrane ruffling, and gyrating movement of the intestine of *C. elegans* [21]. In this study, the group labeled FNDs with epidermal growth factor (EGF) receptors present on the plasma membrane of A431 cells by modifying FNDs with EGF molecules. Then, they calculated the rotational diffusion coefficients of the cell membrane on untreated, EGF-treated (facilitate the assembly of actin filaments), and latrunculin A-treated (disrupted cytoskeletal actin filaments) A-431 cells (Figure 6). The results indicated a correlation between membrane dynamics and intracellular actin filament density. Later, Feng et al. succeeded in 6-D motion (3-D transition and 3-D rotation) tracking of a single FND (200 nm in size) containing ensemble NVCs on a living HeLa cell membrane [68].

Temperature

Various fluorescence-based temperature sensors have been developed to investigate the biological significance of temperature, including dyes, polymers, proteins, and quantum dots [69-71]. These sensors contributed to finding an unexpected distribution of intracellular temperature that is highly inhomogeneous with a variation of more than 1°C. Nevertheless, concerns over the robustness of the sensors against environmental factors (pH, ion concentration, viscosity, and molecular interactions) have been claimed by Baffou et al. Because FND temperature sensors are barely influenced by these environmental factors, carrying out intracellular temperature sensing using FND is indispensable for understanding the link between temperature and cellular functions.

Precise measurements of the local temperature in living systems using FNDs were reported by Kucsko et al.[72] To minimize measurement times, instead of measuring the entire ODMR spectrum, they monitored temperature changes at four points within the ODMR spectrum, which allowed for 4-s temperature measurements with a precision of 0.1 K in HeLa cells. Temperature sensing has also been performed for primary cortical neurons by Simpson et al. [73], and for adipose tissue-derived stem cells by Yukawa et al. [74]. The latter study showed that intracellular temperature influences growth factor production and the degree of differentiation into adipocytes and osteocytes. Recently, Fujiwara et al. performed temperature measurements in *C. elegans* [75]. Because FNDs move quickly inside *C. elegans*, the group developed a fast particle-tracking algorithm. In addition, to exclude artifacts caused by fluorescence intensity fluctuations arising from the body structure of the worm, they also established an error-correction filter. The resulting system allows for real-time temperature measurements using mobile FNDs inside living adult *C. elegans* with a precision of approximately ±0.22°C. This system was successfully employed to determine the internal temperatures of worms under pharmacological treatments using a mitochondrial uncoupler (carbonyl cyanidep-trifluoromethoxyphenylhydrazone (FCCP)) meant to induce non-shivering thermogenesis (Figure 7).
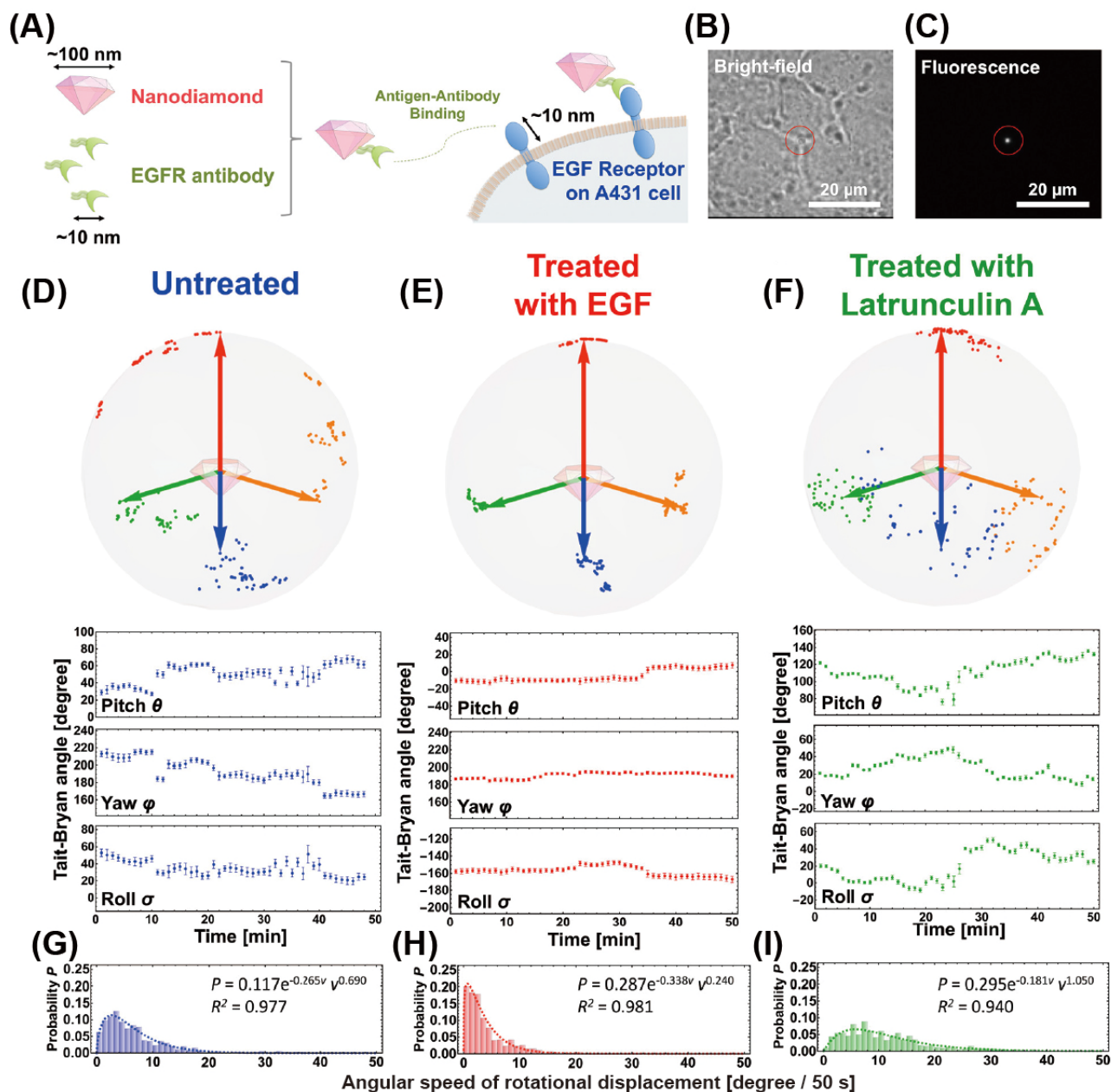
Figure 6 Membrane fluctuations of A431 cells correlate with density of the cytoskeleton. (A) Antigen-antibody association between a nanodiamond and an EGF receptor (schematic). (B,C) Bright-field (B) and selective imaging protocol (SIP). (C) images of nanodiamond-attached A431 cells. (D−F) Typical rotational motion of nanodiamonds on the membrane of untreated (D), EGF-treated (E), and latrunculin A-treated (F) A431 cells. Upper panels show the observed directions of the N−V axes. The directions of the N−V axes at each time point are indicated by the corresponding colored dots on the unit spheres. Lower panels show the time courses of the Tait−Bryan angles. (G−I) Histograms of the frequency of angular speeds of the rotational displacement of N−V axes in nanodiamonds on untreated (G), EGF-treated (H), and latrunculin A-treated (I) A431 cells at each measurement step. Each histogram shows the total data of three independent experiments conducted using different cells under the same conditions. Modified with permission from Ref 21.
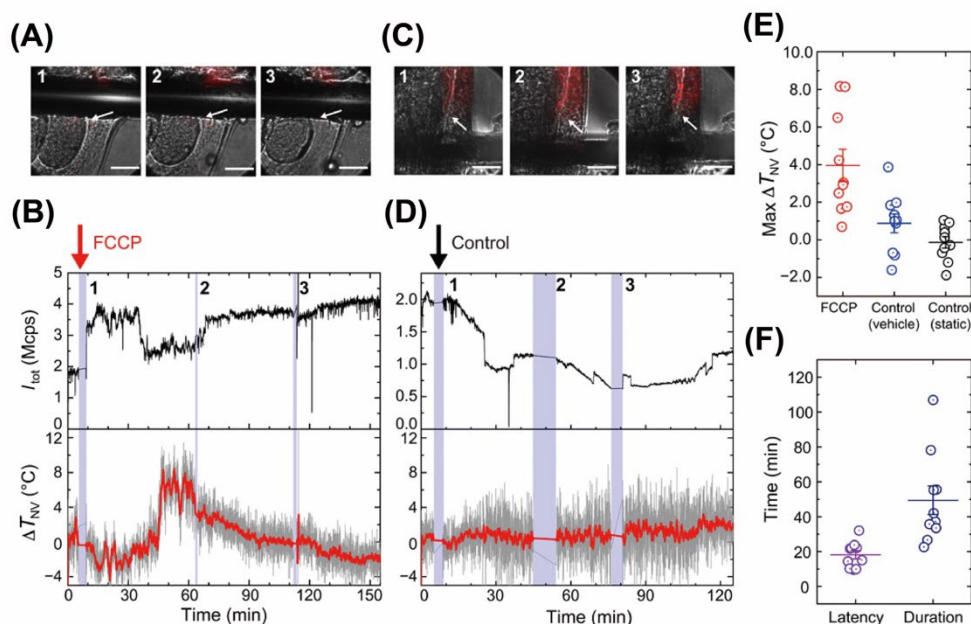
Figure 7 (A and C) Merged photos of FNDs during FCCP stimulation (60 µM) and vehicle control experiments. Images in red and gray represent FND fluorescence and bright field, respectively. The numbers in the upper left-hand corner of each image correspond to specific times at which each picture captured during measurements shown in (B) and (D). Scale bars, 20 µm. (B and D) I_{tot} (top) and ΔT_{NV} (bottom) during FCCP stimulation and vehicle control experiments. The blue shaded regions represent periods when no temperature measurements were performed and in which the photographs in (A) and (C) were obtained. ΔT_{NV} was calculated using the equation $dD/dT = -65.4$ kHz C^{-1} for both types of experiments. (E) Statistical plots of the maximum ΔT_{NV} for FCCP stimulation (red), vehicle control (blue), and static control (black, no solution added). n = 10 for all data. Mean values ± SE were 4.0 ± 0.9, 0.9 ± 0.5, and −0.1 ± 0.3 °C for the FCCP, vehicle control, and static control experiments, respectively. All measurements were performed at a constant temperature of 23 °C with fluctuations of less than 0.25 °C. Probed NDs were located within 20 µm of the antenna, with a mean distance of 8.9 µm. (F) The latency and durations of responses to increased temperature responses of ΔT_{NV} for the FCCP stimulus, whose means ± SEs of 18.1 ± 2.3 and 49.4 ± 8.22 min, respectively. Modified with permission from Ref 75.

Thermal Conductivity

While many studies have focused on intracellular temperatures, few have reported on how heat travels within the cell, that is, thermal conductivity. Heat released from the inside of the cell is transmitted through the cell and ultimately maintains body temperature. Thus, it is important to understand the thermal conductivity of cells to clarify how heat affects surrounding biomolecules and chemical reactions. The thermal conductivity of cells has before now been considered equivalent to that of water [76,77]. However, it is questionable to simply assume that the intracellular environment is watery, because there are many biomolecules and boundary structures within cells. Hence, a method for measuring intracellular thermal conductivity had to be developed.

Because PDA shows a photothermal effect, PDA-coated FND functions as a two-in-one heater/thermometer, which is applicable to thermal conductivity measurements (Figure 8A and B) [22]. The system for thermal conductivity measurement is simple: in media with high thermal conductivities, the nanodiamonds did not become very hot because heat escaped quickly, but in an environment of low thermal conductivity, the nanodiamonds became hotter. Therefore, by monitoring the laser-induced heat, the thermal conductivity of the surrounding environment could be calculated (Figure 8C). Indeed, temperature increases in air, water, and oil are markedly correlated with the literature values of thermal conductivity (Figure 8D). The intracellular thermal conductivities of HeLa and MCF-7 cells were subsequently examined, with the mean conductivities of two separate cell lines being 0.11 ± 0.04 Wm^{-1} K^{-1} (95% confidence) with similar measurement accuracies, which were significantly smaller than that of water (Figure 8D). The group remarked that it was necessary to accurately locate where the temperature was measured to identify the source of the intracellular thermal conductivity. In parallel with this study, Song et al., measured cellular thermal conductivity by monitoring the temperature-dependent changes of the intracellular refractive index induced by optically heated gold nanoparticles. The group reported the intracellular thermal conductivity to be 0.31 Wm^{-1} K^{-1} with a large heterogeneity [78]. This value is

significantly distinct from the one from Sotoma et al. Suzuki and Plakhotnik speculated the different values of thermal conductivities from the two groups are due to the fundamentally different methodologies; while Sotoma et al. measured a steady-state value of temperature, Song et al. pursued measurements of a transient-time [79]. Very recently, Lu et al. established a blue-light-excitable genetically encoded temperature indicator (B-gTEMP) that can measure temperature at a time resolution of 155 μs [80]. B-gTEMP was introduced into a cell and the heat propagation in the cell from photoirradiated carbon nanotubes that were placed outside the cell was measured. The thermal diffusivity was then calculated to be 2.7×10^{-8} m^2 s^{-1}, which is 5.3-fold lower than that of pure water. This value corresponds to 0.11 Wm^{-1} K^{-1} in terms of thermal conductivity under a certain reasonable assumption.
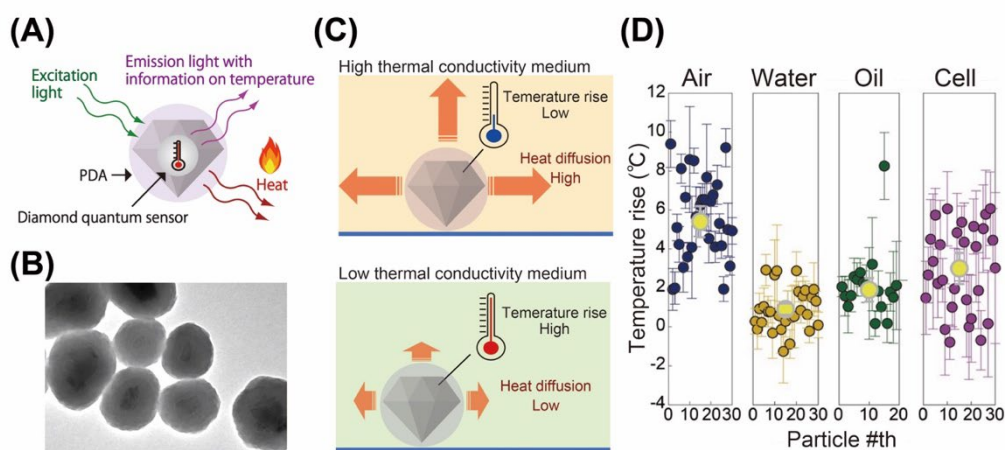

Figure 8 (A) Schematic illustration of dual functional PDA-coated FNDs (FND-PDA) prepared from FNDs. PDA-FNDs function as a luminescent nanothermometer, while PDA releases heat in a light-dependent manner. (B) TEM images of FND-PDA. Images are 751 × 534 nm. (C) Conceptual illustration showing how FND-PDA works as a sensor for thermal conductivity. (D) Plots and error bars indicating $\Delta T \pm$ standard deviation for each particle in different environments measured when increasing laser power from 7.3 to 25 mW. Modified with permission from Ref 22.

Conclusion and Outlook

Measuring physical parameters in the nanometric region is becoming increasingly important for understanding biological systems. It has been reported that several materials, such as dyes, polymers, proteins, and nanoparticles, can be used for biological sensing applications [69,70,81]. Among them, FNDs have a unique structure in which the NVCs that act as actual sensors are embedded deep inside the diamond crystal structure; thus, their thermal sensing is free from environmental fluctuations, which allows for highly accurate temperature sensing [17]. In addition, an FND is one of the few sensors that can measure the temperature with a single particle. Single-particle measurement also minimizes the influence of the concentration of the probe itself on sensing. The study of temperature and thermal conductivity in living organisms is expected to approach the core of thermal biology, such as the principles and significance of body temperature maintenance in thermostatic animals.

Furthermore, FNDs can be used for super-resolution, Raman, cathodoluminescence, correlative light and electron microscopy, and magnetic resonance imaging, which allow multimodal imaging/sensing applications. The potential of FND for biosensing is wide and thus will deliver a new concept of understanding life activity in terms of physical quantity. However, although FNDs have the potential to measure the temperature, magnetic field, electric field, magnetic molecules, radicals, and pH inside single cells, there are limited examples of successful quantitative measurements of these parameters in living cells. To address the biological enigma that can only be answered by the use of this quantum sensor, several important issues must be overcome.

The size of FNDs currently in general use is 50–100 nm which is significantly larger than that of biomolecules. It is technically possible to produce a single-digit nanometer-sized diamond; however, it becomes difficult to measure fluorescence and ODMR signals from such tiny diamonds. To capture the movement of a single protein molecule or to measure physical quantities in the vicinity of an organelle, it is necessary to establish a synthesis technique to produce smaller FNDs that emit large fluorescence and ODMR signals. In addition, the inhomogeneity of the ODMR signal of FNDs is problematic. The size, shape, crystal strain, impurity content, and number of NV centers in the crystals are highly inhomogeneous from particle to particle. Therefore, calibration lines must be recorded for each FND of interest, and the errors are significant. New fabrication methods and novel surface functionalization techniques may help overcome these

challenges. Another issue is the technology used to transport FNDs to specific sites in the cell, such as the nucleus and mitochondria. Although labeling of biomolecules exposed outside the cell membrane, such as membrane proteins, has already been achieved, the hurdle is higher when it comes to biomolecules inside the cell, and highly selective labeling has yet to be achieved. Development of a technique to transport FND inside cells and organelle-targeting strategies is anticipated.

To achieve intracellular quantum sensing using FNDs, it is necessary to integrate a wide range of knowledge and technologies, including materials science for making FNDs, organic chemistry for surface control, quantum science for spin manipulation, and the development of ODMR microscopy, along with biological expertise. We hope that the quantum sensing of cells by FND will lead to new insights into biological systems through the multifaceted participation of various researchers in the future.

Conflict of Interest

The authors declare that there is no conflict of interest.

Author Contributions

S.S. wrote the manuscript with H.O. and S.C. under the supervision of Y.H.

Acknowledgements

References

[1] Degen, C. L., Reinhard, F., Cappellaro, P. Quantum sensing. Rev. Mod. Phys. 89, 035002 (2017). https://doi.org/10.1103/RevModPhys.89.035002

[2] Schirhagl, R., Chang, K., Loretz, M., Degen, C. L. Nitrogen-vacancy centers in diamond: Nanoscale sensors for physics and biology. Annu. Rev. Phys. Chem. 65, 83–105 (2014). https://doi.org/10.1146/annurev-physchem-040513-103659

[3] Ho, K. O., Wong, K. C., Leung, M. Y., Pang, Y. Y., Leung, W. K., Yip, K. Y., et al. Recent developments of quantum sensing under pressurized environment using the nitrogen vacancy (NV) center in diamond. J. Appl. Phys. 129, 241101 (2021). https://doi.org/10.1063/5.0052233

[4] Yu, S. J., Kang, M. W., Chang, H. C., Chen, K. M., Yu, Y. C. Bright fluorescent nanodiamonds: No photobleaching and low cytotoxicity. J. Am. Chem. Soc. 127, 17604–17605 (2005). https://doi.org/10.1021/ja0567081

[5] Hui, Y. Y., Hsiao, W. W.-W., Haziza, S., Simonneau, M., Treussart, F., Chang, H.-C. Single particle tracking of fluorescent nanodiamonds in cells and organisms. Curr. Opin. Solid State Mater. Sci. 21, 35–42 (2017). https://doi.org/10.1016/j.cossms.2016.04.002

[6] Hsiao, W. W., Hui, Y. Y., Tsai, P. C., Chang, H. C. Fluorescent nanodiamond: A versatile tool for long-term cell tracking, super-resolution imaging, and nanoscale temperature sensing. Acc. Chem. Res. 49, 400–407 (2016). https://doi.org/10.1021/acs.accounts.5b00484

[7] Chipaux, M., van der Laan, K. J., Hemelaar, S. R., Hasani, M., Zheng, T., Schirhagl, R. Nanodiamonds and their applications in cells. Small 14, e1704263 (2018). https://doi.org/10.1002/smll.201704263

[8] Zhang, T., Pramanik, G., Zhang, K., Gulka, M., Wang, L., Jing, J., et al. Toward quantitative bio-sensing with nitrogen-vacancy center in diamond. ACS Sens. 6, 2077–2107 (2021). https://doi.org/10.1021/acssensors.1c00415

[9] Wu, Y., Weil, T. Recent developments of nanodiamond quantum sensors for biological applications. Adv. Sci. (Weinh) e2200059 (2022). https://doi.org/10.1002/advs.202200059

[10] Gruber, A., Drabenstedt, A., Tietz, C., Fleury, L., Wrachtrup, J., von Borczyskowski, C. Scanning confocal optical microscopy and magnetic resonance on single defect centers. Science 276, 2012–2014 (1997). https://doi.org/10.1126/science.276.5321.2012

[11] Fujisaku, T., Tanabe, R., Onoda, S., Kubota, R., Segawa, T. F., So, F. T., et al. pH nanosensor using electronic spins in diamond. ACS Nano 13, 11726–11732 (2019). https://doi.org/10.1021/acsnano.9b05342

[12] Ermakova, A., Pramanik, G., Cai, J. M., Algara-Siller, G., Kaiser, U., Weil, T., et al. Detection of a few metallo-protein molecules using color centers in nanodiamonds. Nano Lett. 13, 3305–3309 (2013). https://doi.org/10.1021/nl4015233

[13] Barton, J., Gulka, M., Tarabek, J., Mindarava, Y., Wang, Z., Schimer, J., et al. Nanoscale dynamic readout of a chemical redox process using radicals coupled with nitrogen-vacancy centers in nanodiamonds. ACS Nano 14, 12938–12950 (2020). https://doi.org/10.1021/acsnano.0c04010

[14] Nie, L., Nusantara, A. C., Damle, V. G., Sharmin, R., Evans, E. P. P., Hemelaar, S. R., et al. Quantum monitoring of cellular metabolic activities in single mitochondria. Sci. Adv. 7, eabf0573 (2021). https://doi.org/10.1126/sciadv.abf0573

[15] Nie, L., Nusantara, A. C., Damle, V. G., Baranov, M. V., Chipaux, M., Reyes-San-Martin, C., et al. Quantum sensing of free radicals in primary human dendritic cells. Nano Lett. 22, 1818–1825 (2022). https://doi.org/10.1021/acs.nanolett.1c03021

[16] Miller, B. S., Bezinge, L., Gliddon, H. D., Huang, D., Dold, G., Gray, E. R., et al. Spin-enhanced nanodiamond biosensing for ultrasensitive diagnostics. Nature 587, 588–593 (2020). https://doi.org/10.1038/s41586-020-2917-1

[17] Sekiguchi, T., Sotoma, S., Harada, Y. Fluorescent nanodiamonds as a robust temperature sensor inside a single cell. Biophys. Physicobiol. 15, 229–234 (2018). https://doi.org/10.2142/biophysico.15.0_229

[18] Sotoma, S., Terada, D., Segawa, T. F., Igarashi, R., Harada, Y., Shirakawa, M. Enrichment of ODMR-active nitrogen-vacancy centres in five-nanometre-sized detonation-synthesized nanodiamonds: Nanoprobes for temperature, angle and position. Sci. Rep. 8, 5463 (2018). https://doi.org/10.1038/s41598-018-23635-5

[19] Sotoma, S., Epperla, C. P., Chang, H.-C. Diamond nanothermometry. ChemNanoMat 4, 15–27 (2018). https://doi.org/10.1002/cnma.201700257

[20] Igarashi, R., Yoshinari, Y., Yokota, H., Sugi, T., Sugihara, F., Ikeda, K., et al. Real-time background-free selective imaging of fluorescent nanodiamonds in vivo. Nano Lett. 12, 5726–5732 (2012). https://doi.org/10.1021/nl302979d

[21] Igarashi, R., Sugi, T., Sotoma, S., Genjo, T., Kumiya, Y., Walinda, E., et al. Tracking the 3D rotational dynamics in nanoscopic biological systems. J Am Chem Soc 142, 7542–7554 (2020). https://doi.org/10.1021/jacs.0c01191

[22] Sotoma, S., Zhong, C., Kah, J. C. Y., Yamashita, H., Plakhotnik, T., Harada, Y., et al. In situ measurements of intracellular thermal conductivity using heater-thermometer hybrid diamond nanosensors. Sci. Adv. 7, eabd7888 (2021). https://doi.org/10.1126/sciadv.abd7888

[23] Sotoma, S., Harada, Y. Composite quantum sensors based on fluorescent nanodiamonds for intracellular controlled heating in living cells. ACS Appl. Nano Mater. 4, 3969–3976 (2021). https://doi.org/10.1021/acsanm.1c00334

[24] Doherty, M. W., Manson, N. B., Delaney, P., Jelezko, F., Wrachtrup, J., Hollenberg, L. C. L. The nitrogen-vacancy colour centre in diamond. Phys. Rep. 528, 1–45 (2013). https://doi.org/10.1016/j.physrep.2013.02.001

[25] Jacques, V., Neumann, P., Beck, J., Markham, M., Twitchen, D., Meijer, J., et al. Dynamic polarization of single nuclear spins by optical pumping of nitrogen-vacancy color centers in diamond at room temperature. Phys. Rev. Lett. 102, 057403 (2009). https://doi.org/10.1103/PhysRevLett.102.057403

[26] Jarmola, A., Berzins, A., Smits, J., Smits, K., Prikulis, J., Gahbauer, F., et al. Longitudinal spin-relaxation in nitrogen-vacancy centers in electron irradiated diamond. App. Phys. Lett. 107, 242403 (2015). https://doi.org/10.1063/1.4937489

[27] Gaebel, T., Popa, I., Gruber, A., Domhan, M., Jelezko, F., Wrachtrup, J. Stable single-photon source in the near infrared. New J. Phys. 6, 98 (2004). https://doi.org/10.1088/1367-2630/6/1/098

[28] Chang, Y. R., Lee, H. Y., Chen, K., Chang, C. C., Tsai, D. S., Fu, C. C., et al. Mass production and dynamic imaging of fluorescent nanodiamonds. Nat. Nanotechnol. 3, 284–288 (2008). https://doi.org/10.1038/nnano.2008.99

[29] Bradac, C., Gaebel, T., Naidoo, N., Sellars, M. J., Twamley, J., Brown, L. J., et al. Observation and control of blinking nitrogen-vacancy centres in discrete nanodiamonds. Nat. Nanotechnol. 5, 345–349 (2010). https://doi.org/10.1038/nnano.2010.56

[30] Barbiero, M., Castelletto, S., Gan, X., Gu, M. Spin-manipulated nanoscopy for single nitrogen-vacancy center localizations in nanodiamonds. Light Sci. Appl. 6 (2017). https://doi.org/10.1038/lsa.2017.85

[31] Jelezko, F., Wrachtrup, J. Single defect centres in diamond: A review. Phys. Status Solidi A 203, 3207–3225 (2006). https://doi.org/10.1002/pssa.200671403

[32] Staudacher, T., Shi, F., Pezzagna, S., Meijer, J., Du, J., Meriles, C. A., et al. Nuclear magnetic resonance spectroscopy on a (5-nanometer)^3 sample volume. Science 339, 561–563 (2013). https://doi.org/10.1126/science.1231675

[33] Geiselmann, M., Juan, M. L., Renger, J., Say, J. M., Brown, L. J., de Abajo, F. J., et al. Three-dimensional optical manipulation of a single electron spin. Nat. Nanotechnol. 8, 175–179 (2013). https://doi.org/10.1038/nnano.2012.259

[34] McGuinness, L. P., Yan, Y., Stacey, A., Simpson, D. A., Hall, L. T., Maclaurin, D., et al. Quantum measurement and orientation tracking of fluorescent nanodiamonds inside living cells. Nat. Nanotechnol. 6, 358–363 (2011).

https://doi.org/10.1038/nnano.2011.64

[35] Acosta, V. M., Bauch, E., Ledbetter, M. P., Waxman, A., Bouchard, L. S., Budker, D. Temperature dependence of the nitrogen-vacancy magnetic resonance in diamond. Phys. Rev. Lett. 104, 070801 (2010). https://doi.org/10.1103/PhysRevLett.104.070801

[36] Chen, X. D., Dong, C. H., Sun, F. W., Zou, C. L., Cui, J. M., Han, Z. F., et al. Temperature dependent energy level shifts of nitrogen-vacancy centers in diamond. Appl. Phys. Lett. 99, 161903 (2011). https://doi.org/10.1063/1.3652910

[37] Plakhotnik, T., Aman, H., Chang, H. C. All-optical single-nanoparticle ratiometric thermometry with a noise floor of 0.3 K Hz$^{-1/2}$. Nanotechnology 26, 245501 (2015). https://doi.org/10.1088/0957-4484/26/24/245501

[38] Hui, Y. Y., Chen, O. Y., Azuma, T., Chang, B.-M., Hsieh, F.-J., Chang, H.-C. All-optical thermometry with nitrogen-vacancy centers in nanodiamond-embedded polymer films. J. Phys. Chem. C 123, 15366–15374 (2019). https://doi.org/10.1021/acs.jpcc.9b04496

[39] Sotoma, S., Igarashi, R., Iimura, J., Kumiya, Y., Tochio, H., Harada, Y., et al. Suppression of nonspecific protein–nanodiamond adsorption enabling specific targeting of nanodiamonds to biomolecules of interest. Chem. Lett. 44, 354–356 (2015). https://doi.org/10.1246/cl.141036

[40] Neburkova, J., Vavra, J., Cigler, P. Coating nanodiamonds with biocompatible shells for applications in biology and medicine. Curr. Opin. Solid State Mater. Sci. 21, 43–53 (2017). https://doi.org/10.1016/j.cossms.2016.05.008

[41] Sotoma, S., Hsieh, F.-J., Chang, H.-C. Biohybrid fluorescent nanodiamonds as dual-contrast markers for light and electron microscopies. J. Chin. Chem. Soc. 65, 1136–1146 (2018). https://doi.org/10.1002/jccs.201800157

[42] Lee, J. W., Lee, S., Jang, S., Han, K. Y., Kim, Y., Hyun, J., et al. Preparation of non-aggregated fluorescent nanodiamonds (FNDs) by non-covalent coating with a block copolymer and proteins for enhancement of intracellular uptake. Mol. Biosyst. 9, 1004–1011 (2013). https://doi.org/10.1039/c2mb25431j

[43] Tzeng, Y. K., Faklaris, O., Chang, B. M., Kuo, Y., Hsu, J. H., Chang, H. C. Superresolution imaging of albumin-conjugated fluorescent nanodiamonds in cells by stimulated emission depletion. Angew. Chem. Int. Ed Engl. 50, 2262–2265 (2011). https://doi.org/10.1002/anie.201007215

[44] Epperla, C. P., Mohan, N., Chang, C. W., Chen, C. C., Chang, H. C. Nanodiamond-mediated intercellular transport of proteins through membrane tunneling nanotubes. Small 11, 6097–6105 (2015). https://doi.org/10.1002/smll.201502089

[45] Chang, B.-M., Lin, H.-H., Su, L.-J., Lin, W.-D., Lin, R.-J., Tzeng, Y.-K., et al. Highly fluorescent nanodiamonds protein-functionalized for cell labeling and targeting. Adv. Func. Mater. 23, 5737–5745 (2013). https://doi.org/10.1002/adfm.201301075

[46] Su, L. J., Lin, H. H., Wu, M. S., Pan, L., Yadav, K., Hsu, H. H., et al. Intracellular delivery of luciferase with fluorescent nanodiamonds for dual-modality imaging of human stem cells. Bioconjug. Chem. 30, 2228–2237 (2019). https://doi.org/10.1021/acs.bioconjchem.9b00458

[47] Zhang, X. Q., Chen, M., Lam, R., Xu, X., Osawa, E., Ho, D. Polymer-functionalized nanodiamond platforms as vehicles for gene delivery. ACS Nano 3, 2609–2616 (2009). https://doi.org/10.1021/nn900865g

[48] Chen, M., Zhang, X.-Q., Man, H. B., Lam, R., Chow, E. K., Ho, D. Nanodiamond vectors functionalized with polyethylenimine for siRNA delivery. J. Phys. Chem. Lett. 1, 3167–3171 (2010). https://doi.org/10.1021/jz1013278

[49] Petrakova, V., Benson, V., Buncek, M., Fiserova, A., Ledvina, M., Stursa, J., et al. Imaging of transfection and intracellular release of intact, non-labeled DNA using fluorescent nanodiamonds. Nanoscale 8, 12002–12012 (2016). https://doi.org/10.1039/c6nr00610h

[50] Hsieh, F. J., Chen, Y. W., Huang, Y. K., Lee, H. M., Lin, C. H., Chang, H. C. Correlative light-electron microscopy of lipid-encapsulated fluorescent nanodiamonds for nanometric localization of cell surface antigens. Anal. Chem. 90, 1566–1571 (2018). https://doi.org/10.1021/acs.analchem.7b04549

[51] Sotoma, S., Hsieh, F. J., Chen, Y. W., Tsai, P. C., Chang, H. C. Highly stable lipid-encapsulation of fluorescent nanodiamonds for bioimaging applications. Chem. Commun. (Camb) 54, 1000–1003 (2018). https://doi.org/10.1039/c7cc08496j

[52] Vavra, J., Rehor, I., Rendler, T., Jani, M., Bednar, J., Baksh, M. M., et al. Supported lipid bilayers on fluorescent nanodiamonds: A structurally defined and versatile coating for bioapplications. Adv. Func. Mater. 28, 1803406 (2018). https://doi.org/10.1002/adfm.201803406

[53] Morita, A., Hamoh, T., Martinez, F. P. P., Chipaux, M., Sigaeva, A., Mignon, C., et al. The fate of lipid-coated and uncoated fluorescent nanodiamonds during cell division in yeast. Nanomaterials (Basel) 10, 516 (2020). https://doi.org/10.3390/nano10030516

[54] Zeng, Y., Liu, W., Wang, Z., Singamaneni, S., Wang, R. Multifunctional surface modification of nanodiamonds based on dopamine polymerization. Langmuir 34, 4036–4042 (2018). https://doi.org/10.1021/acs.langmuir.8b00509

[55] Jung, H.-S., Cho, K.-J., Seol, Y., Takagi, Y., Dittmore, A., Roche, P. A., et al. Polydopamine encapsulation of fluorescent nanodiamonds for biomedical applications. Adv. Func. Mater. 28, 1801252 (2018). https://doi.org/10.1002/adfm.201801252

[56] Bumb, A., Sarkar, S. K., Billington, N., Brechbiel, M. W., Neuman, K. C. Silica encapsulation of fluorescent nanodiamonds for colloidal stability and facile surface functionalization. J. Am. Chem. Soc. 135, 7815–7818 (2013). https://doi.org/10.1021/ja4016815

[57] Rehor, I., Slegerova, J., Kucka, J., Proks, V., Petrakova, V., Adam, M. P., et al. Fluorescent nanodiamonds embedded in biocompatible translucent shells. Small 10, 1106–1115 (2014). https://doi.org/10.1002/smll.201302336

[58] Chu, Z., Zhang, S., Zhang, B., Zhang, C., Fang, C. Y., Rehor, I., et al. Unambiguous observation of shape effects on cellular fate of nanoparticles. Sci. Rep. 4, 4495 (2014). https://doi.org/10.1038/srep04495

[59] Khan, M., Huck, W. T. S. Hyperbranched polyglycidol on Si/SiO$_2$ surfaces via surface-initiated polymerization. Macromolecules 36, 5088–5093 (2003). https://doi.org/10.1021/ma0340762

[60] Zhao, L., Takimoto, T., Ito, M., Kitagawa, N., Kimura, T., Komatsu, N. Chromatographic separation of highly soluble diamond nanoparticles prepared by polyglycerol grafting. Angew. Chem. Int. Ed Engl. 50, 1388–1392 (2011). https://doi.org/10.1002/anie.201006310

[61] Sotoma, S., Shirakawa, M. Monodispersed colloidal solutions of surface-modified detonation-synthesized nanodiamonds and their aggregation resistance. Chem. Lett. 45, 697–699 (2016). https://doi.org/10.1246/cl.160250

[62] Hsieh, F. J., Sotoma, S., Lin, H. H., Cheng, C. Y., Yu, T. Y., Hsieh, C. L., et al. Bioorthogonal fluorescent nanodiamonds for continuous long-term imaging and tracking of membrane proteins. ACS Appl. Mater. Interfaces 11, 19774–19781 (2019). https://doi.org/10.1021/acsami.9b03640

[63] Torelli, M. D., Rickard, A. G., Backer, M. V., Filonov, D. S., Nunn, N. A., Kinev, A. V., et al. Targeting fluorescent nanodiamonds to vascular endothelial growth factor receptors in tumor. Bioconjug. Chem. 30, 604–613 (2019). https://doi.org/10.1021/acs.bioconjchem.8b00803

[64] Zhao, L., Xu, Y.-H., Qin, H., Abe, S., Akasaka, T., Chano, T., et al. Platinum on nanodiamond: A promising prodrug conjugated with stealth polyglycerol, targeting peptide and acid-responsive antitumor drug. Adv. Func. Mater. 24, 5348–5357 (2014). https://doi.org/10.1002/adfm.201304298

[65] Terada, D., Sotoma, S., Harada, Y., Igarashi, R., Shirakawa, M. One-Pot Synthesis of Highly Dispersible Fluorescent Nanodiamonds for Bioconjugation. Bioconjug. Chem. 29, 2786–2792 (2018). https://doi.org/10.1021/acs.bioconjchem.8b00412

[66] Sotoma, S., Hsieh, F. J., Chang, H. C. Single-step metal-free grafting of cationic polymer brushes on fluorescent nanodiamonds. Materials (Basel) 11, 1479 (2018). https://doi.org/10.3390/ma11081479

[67] Wang, Y., Cai, E., Sheung, J., Lee, S. H., Teng, K. W., Selvin, P. R. Fluorescence imaging with one-nanometer accuracy (FIONA). J. Vis. Exp. 51774 (2014). https://doi.org/10.3791/51774

[68] Feng, X., Leong, W. H., Xia, K., Liu, C. F., Liu, G. Q., Rendler, T., et al. Association of nanodiamond rotation dynamics with cell activities by translation-rotation tracking. Nano Lett. 21, 3393–3400 (2021). https://doi.org/10.1021/acs.nanolett.0c04864

[69] Nakano, M., Nagai, T. Thermometers for monitoring cellular temperature. Journal of Photochemistry and Photobiology C: Photochemistry Reviews 30, 2–9 (2017). https://doi.org/10.1016/j.jphotochemrev.2016.12.001

[70] Okabe, K., Sakaguchi, R., Shi, B., Kiyonaka, S. Intracellular thermometry with fluorescent sensors for thermal biology. Pflugers Arch. 470, 717–731 (2018). https://doi.org/10.1007/s00424-018-2113-4

[71] Feng, G., Zhang, H., Zhu, X., Zhang, J., Fang, J. Fluorescence thermometers: Intermediation of fundamental temperature and light. Biomater. Sci. 10, 1855–1882 (2022). https://doi.org/10.1039/d1bm01912k

[72] Kucsko, G., Maurer, P. C., Yao, N. Y., Kubo, M., Noh, H. J., Lo, P. K., et al. Nanometre-scale thermometry in a living cell. Nature 500, 54–58 (2013). https://doi.org/10.1038/nature12373

[73] Simpson, D. A., Morrisroe, E., McCoey, J. M., Lombard, A. H., Mendis, D. C., Treussart, F., et al. Non-neurotoxic nanodiamond probes for intraneuronal temperature mapping. ACS Nano 11, 12077–12086 (2017). https://doi.org/10.1021/acsnano.7b04850

[74] Yukawa, H., Fujiwara, M., Kobayashi, K., Kumon, Y., Miyaji, K., Nishimura, Y., et al. A quantum thermometric sensing and analysis system using fluorescent nanodiamonds for the evaluation of living stem cell functions according to intracellular temperature. Nanoscale Adv. 2, 1859–1868 (2020). https://doi.org/10.1039/d0na00146e

[75] Fujiwara, M., Sun, S., Dohms, A., Nishimura, Y., Suto, K., Takezawa, Y., et al. Real-time nanodiamond thermometry probing in vivo thermogenic responses. Sci. Adv. 6, eaba9636 (2020). https://doi.org/10.1126/sciadv.aba9636

[76] Kyoo Park, B., Yi, N., Park, J., Kim, D. Thermal conductivity of single biological cells and relation with cell viability. Appl. Phys. Lett. 102, 203702 (2013). https://doi.org/10.1063/1.4807471

[77] Baffou, G., Rigneault, H., Marguet, D., Jullien, L. A critique of methods for temperature imaging in single cells. Nat. Methods 11, 899–901 (2014). https://doi.org/10.1038/nmeth.3073

[78] Song, P., Gao, H., Gao, Z., Liu, J., Zhang, R., Kang, B., et al. Heat transfer and thermoregulation within single cells revealed by transient plasmonic imaging. Chem 7, 1569–1587 (2021). https://doi.org/10.1016/j.chempr.2021.02.027

[79] Suzuki, M., Plakhotnik, T. Opportunities for hybrid diamond nanosensors targeting photothermal applications in biological systems. Appl. Phys. Lett. 119, 190502 (2021). https://doi.org/10.1063/5.0063089

[80] Lu, K., Wazawa, T., Sakamoto, J., Vu, C. Q., Nakano, M., Kamei, Y., et al. Intracellular heat transfer and thermal property revealed by kilohertz temperature imaging with a genetically encoded nanothermometer. Nano Lett. 22, 5698–5707 (2022). https://doi.org/10.1021/acs.nanolett.2c00608

[81] Holzinger, M., Le Goff, A., Cosnier, S. Nanomaterials for biosensing applications: A review. Front. Chem. 2, 63 (2014). https://doi.org/10.3389/fchem.2014.00063